

in a coincidence pattern not containing any intensity zeroes. Such a coincidence pattern would also be observed if a shifted hologram together with a mono-mode detector were not able to analyse for superposition states.

An entangled state represents correctly both the correlation of the eigenmodes and the correlations of their superpositions. Having experimentally confirmed the quantum superposition for $l = 0$ and $l = \pm 2$, it is reasonable to expect the quantum superposition will also occur for the other states. Nevertheless, ultimate confirmation of entanglement will be a Bell inequality experiment generalized to more states²⁵. Such an experiment will be a major experimental challenge, and we are preparing to perform it.

For a pump beam with zero angular momentum, the emitted state must then be represented by

$$\psi = C_{0,0}|0\rangle|0\rangle + C_{1,-1}|1\rangle - 1\rangle + C_{-1,1}| - 1\rangle|1\rangle + C_{2,-2}|2\rangle - 2\rangle + C_{-2,2}| - 2\rangle|2\rangle + \dots \quad (1)$$

as the LG modes form an infinite dimensional basis. Here the numbers in the brackets represent the indices l of the LG modes, and the $C_{i,j}$ denote the corresponding probability amplitude for measuring $|i\rangle|j\rangle$. The state (1) is a multi-dimensional entangled state for two photons, which in general will also contain terms with radial mode index $p \neq 0$. It means neither photon in state (1) possesses a well-defined orbital angular momentum after parametric down-conversion. The measurement of one photon defines its orbital angular momentum state, and projects the second one into the corresponding orbital angular momentum state.

It is conceivable that these states could in the future be extended to multi-dimensional multi-particle entanglement. A growing body of theoretical work calls for entanglement of quantum systems of higher dimensions^{7,8}. These states have applications in quantum cryptography with higher alphabets and in quantum teleportation. As such states increase the flux of information, it is conceivable that they could be important for many other applications in quantum communication and in quantum information. The possibility of using these photon states to drive micromachines, and the application of these states as optical tweezers, make them versatile and potentially suitable for future technologies^{19–21}. □

Received 12 March; accepted 5 June 2001.

- Schrödinger, E. Die gegenwärtige Situation in der Quantenmechanik. *Naturwissenschaften* **23**, 807–812; 823–828; 844–849 (1935).
- Schrödinger, E. Discussion of probability relations between separated systems. *Proc. Camb. Phil. Soc.* **31**, 555–563 (1935).
- Bouwmeester, D., Pan, J.-W., Daniell, M., Weinfurter, H. & Zeilinger, A. Observation of a three-photon Greenberger-Horne-Zeilinger state. *Phys. Rev. Lett.* **82**, 1345–1349 (1999).
- Pan, J.-W., Bouwmeester, D., Daniell, M., Weinfurter, H. & Zeilinger, A. Experimental test of quantum nonlocality in three-photon Greenberger-Horne-Zeilinger entanglement. *Nature* **403**, 515–519 (2000).
- Sackett, C. A. *et al.* Experimental entanglement of four particles. *Nature* **404**, 256–259 (2000).
- Pan, J.-W., Daniell, M., Gasparoni, S., Weihs, G. & Zeilinger, A. Experimental demonstration of four-photon entanglement and high-fidelity teleportation. *Phys. Rev. Lett.* **86**, 4435–4438 (2001).
- DiVincenzo, D. P., More, T., Shor, P. W., Smolin, J. A. & Terhal, B. M. Unextendible product bases, uncompletable product bases and bound entanglement. Preprint quant-ph/9908070 at (<http://xxx.lanl.gov>) (1999).
- Bartlett, S. D., de Guise, H. & Sanders, B. C. Quantum computation with harmonic oscillators. Preprint quant-ph/0011080 at (<http://xxx.lanl.gov>) (2000).
- Bechmann-Pasquinucci, H. & Peres, A. Quantum cryptography with 3-state systems. *Phys. Rev. Lett.* **85**, 3313–3316 (2000).
- Bechmann-Pasquinucci, H. & Tittel, W. Quantum cryptography using larger alphabets. *Phys. Rev. A* **61**, 62308–62313 (2000).
- Bourennane, M., Karlsson, A. & Björk, G. Quantum key distribution using multilevel encoding. *Phys. Rev. A* (in the press).
- Reck, M., Zeilinger, A., Bernstein, H. J. & Bertani, P. Experimental realization of any discrete unitary operator. *Phys. Rev. Lett.* **73**, 58–61 (1994).
- Zukowski, M., Zeilinger, A. & Horne, M. Realizable higher-dimensional two-particle entanglements via multiphoton beam splitters. *Phys. Rev. A* **55**, 2564–2579 (1997).
- Reck, M. *Quantum Interferometry with Multiphotons: Entangled Photons in Optical Fibers*. Thesis, Univ. Innsbruck (1996).
- Arnaut, H. H. & Barbosa, G. A. Orbital and angular momentum of single photons and entangled pairs of photons generated by parametric down-conversion. *Phys. Rev. Lett.* **85**, 286–289 (2000).

16. Franke-Arnold, S., Barnett, S. M., Padgett, M. J. & Allen, L. Two-photon entanglement of orbital angular momentum states. *Phys. Rev. A* (in the press).
17. Allen, L., Beijersbergen, M. W., Spreeuw, R. J. C. & Woerdman, J. P. Orbital angular momentum of light and the transformation of laguerre-gaussian laser modes. *Phys. Rev. A* **45**, 8185–8189 (1992).
18. He, H., Fries, M., Heckenberg, N. & Rubinsztein-Dunlop, H. Direct observation of transfer of angular momentum to absorptive particles from a laser beam with a phase singularity. *Phys. Rev. Lett.* **75**, 826–829 (1995).
19. Simpson, N. B., Dholakia, K., Allen, L. & Padgett, M. J. Mechanical equivalence of spin and orbital angular momentum of light: An optical spanner. *Opt. Lett.* **22**, 52–54 (1997).
20. Galajda, P. & Ormos, P. Complex micromachines produced and driven by light. *Appl. Phys. Lett.* **78**, 249–251 (2001).
21. Frieze, M. E. J., Enger, J., Rubinsztein-Dunlop, H. & Heckenberg, N. Optical angular-momentum transfer to trapped absorbing particles. *Phys. Rev. A* **54**, 1593–1596 (1996).
22. Beijersbergen, M. W., Allen, L., van der Veen, H. E. L. O. & Woerdman, J. P. Astigmatic laser mode converters and transfer of orbital angular momentum. *Opt. Commun.* **96**, 123–132 (1993).
23. Arit, J., Dholakia, K., Allen, L. & Padgett, M. J. The production of multiringed laguerre-gaussian modes by computer-generated holograms. *J. Mod. Opt.* **45**, 1231–1237 (1998).
24. Arit, J., Dholakia, K., Allen, L. & Padgett, M. Parametric down-conversion for light beams possessing orbital angular momentum. *Phys. Rev. A* **59**, 3950–3952 (1999).
25. Kaszlikowski, D., Gnacinski, P., Zukowski, M., Miklaszewski, W. & Zeilinger, A. Violation of local realism by two entangled n-dimensional systems are stronger than for two qubits. *Phys. Rev. Lett.* **85**, 4418–4421 (2000).

Acknowledgements

This work was supported by the Austrian Fonds zur Förderung der wissenschaftlichen Forschung (FWF).

Correspondence and requests for materials should be addressed to A.Z. (e-mail: anton.zeilinger@univie.ac.at).

Superconductivity in the non-magnetic state of iron under pressure

Katsuya Shimizu*†, Tomohiro Kimura*, Shigeyuki Furomoto*, Keiki Takeda*, Kazuyoshi Kontani*, Yoshichika Onuki‡ & Kiichi Amaya*†

* Department of Physical Science, Graduate School of Engineering Science, Osaka University, Toyonaka, Osaka 560-8531, USA

† Research Center for Materials Science at Extreme Conditions, Osaka University, Toyonaka, Osaka 560-8531, Japan

‡ Department of Physics, Graduate School of Science, Osaka University, Osaka 560-0043, Japan

Ferromagnetism and superconductivity are thought to compete in conventional superconductors, although in principle it is possible for any metal to become a superconductor in its non-magnetic state at a sufficiently low temperature. At pressures above 10 GPa, iron is known to transform to a non-magnetic structure^{1,2} and the possibility of superconductivity in this state has been predicted^{3,4}. Here we report that iron does indeed become superconducting at temperatures below 2 K at pressures between 15 and 30 GPa. The transition to the superconducting state is confirmed by both a drop in resistivity and observation of the Meissner effect.

An iron sample with purity of 99.995% (Johnson Matthey) was purified further and degassed by heating close to the melting point in an ultra-high-vacuum chamber. The sample was cut into a rectangular shape of $0.04 \times 0.160 \times 0.07 \text{ mm}^3$ and placed in the sample chamber of a non-magnetic diamond-anvil cell (DAC) made of BeCu alloy. For electrical resistivity measurements the BeCu metal gasket was covered with a thin Al_2O_3 layer for electrical insulation. Electrical resistivity measurements are performed using the a.c. four-terminal method with a typical measuring current of $0.1 \times 10^{-6} \text{ A}$ at low temperatures below 10 K. The sample chamber was filled with NaCl as the pressure-transmitting medium (Fig. 1a). Several ruby chips of less than 0.002 mm in diameter were located around the sample and the applied pressure

was determined by a standard ruby fluorescence method. The pressure was applied and fixed at room temperature, and the DAC was assembled on the mixer of a $^3\text{He}/^4\text{He}$ dilution refrigerator; the temperature dependence of the resistivity of iron was measured at temperatures down to 30 mK.

A small but definite drop in the electrical resistivity was observed at temperatures below 2 K at pressures above 16 GPa. A typical resistivity–temperature (R – T) curve at a pressure of 25 GPa is shown in Fig. 1b. As expected for conventional superconductors, the drop was suppressed and broadened by a large measuring current above 1×10^{-6} A. When we applied an external magnetic field the resistivity drop shifted towards lower temperatures and disappeared at 0.2 T, as shown in Fig. 2. The observed magnetic-field dependence shows that the drop was due to the superconducting transition of the iron sample. The measured critical field for iron is almost ten times larger than that of other superconductors such as rhenium or thallium with similar critical temperatures of about 2 K. The change in the resistivity due to the transition was less than 10%

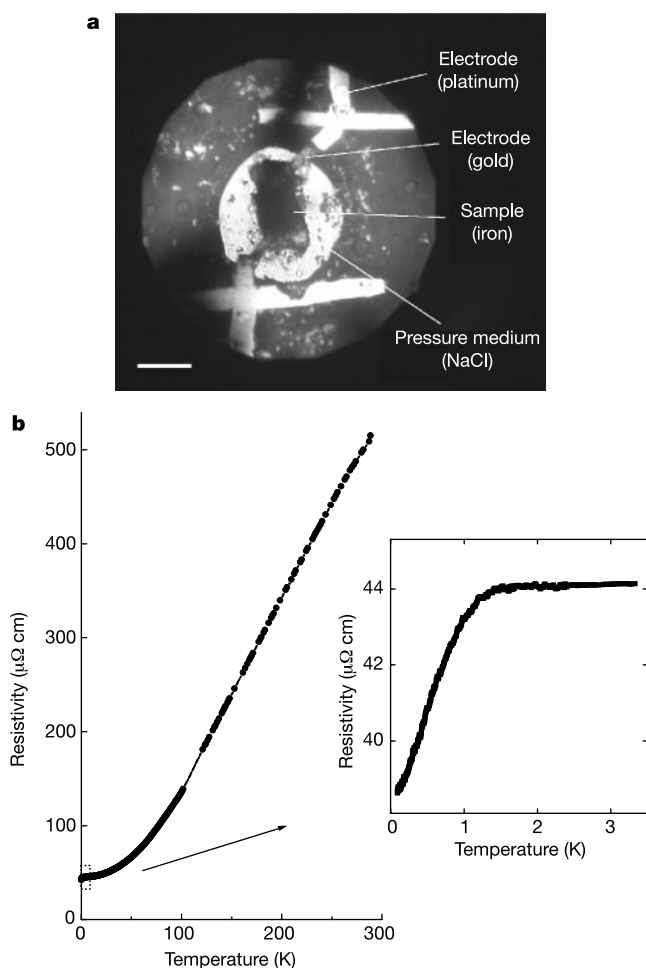


Figure 1 Arrangement of sample in the pressure-cell, and the low-temperature experimental curve of the resistance of iron at 25 GPa. **a**, Photograph showing the configuration of the sample and electrodes on the pressure surface of the diamond anvil. The gold wires, 0.01 mm in diameter, were attached to the sample crystal using micro-spot welding and placed in the sample chamber, which was filled with sodium chloride and connected to a platinum electrode outside the chamber. **b**, Temperature dependence of the electrical resistivity of iron at 25 GPa. A 10% drop in resistivity indicates the onset of superconductivity at around 1.5 K. To our knowledge, no report exists for the superconductivity of gold or platinum, including the pressure-induced case. Nor had we previously detected a superconducting signal from gold or platinum in experiments in this pressure region. Scale bar, 0.1 mm.

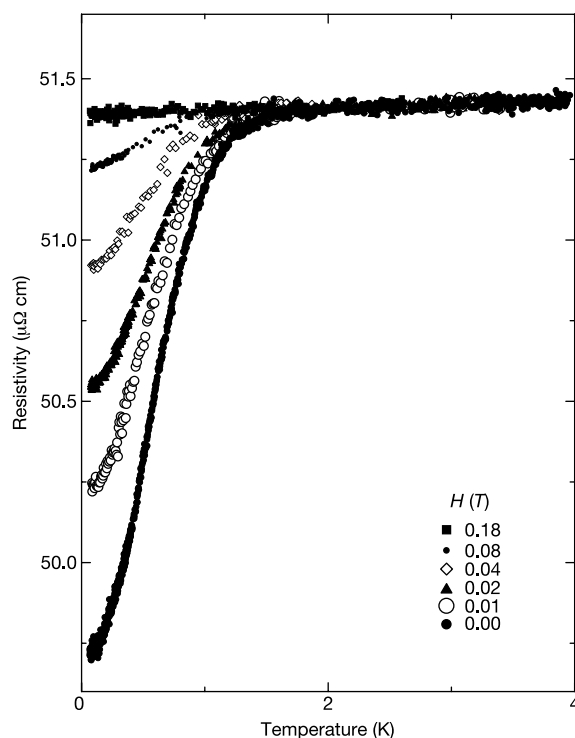


Figure 2 Magnetic-field dependence of the resistance drop of iron for various magnetic fields at 23 GPa. The resistance drop shifts towards lower temperature with increasing applied magnetic field. Above 0.18 T, only the temperature-independent residual resistance value is observed.

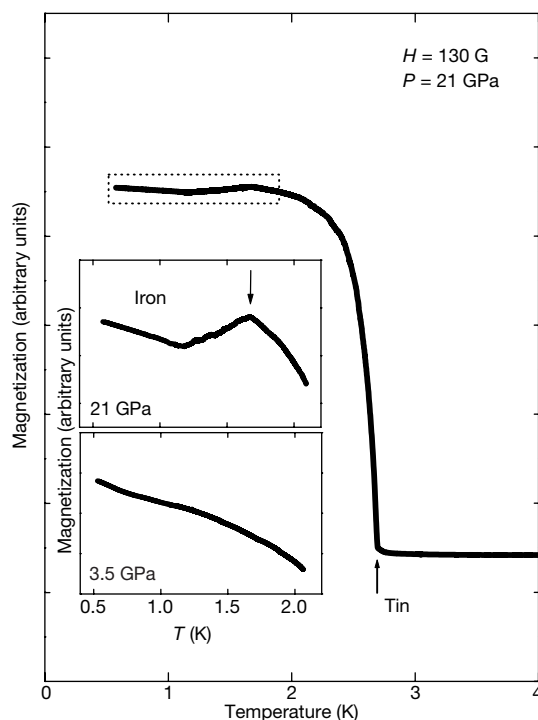


Figure 3 The temperature dependence of the magnetization of iron under pressure obtained by cooling the sample at a magnetic field of 130 G. The signal at 21 GPa (the area enclosed by the dotted line is expanded in the upper inset) shows the appearance of diamagnetism at temperatures below 1.7 K, which is confirmed by the signal given by tin at 2.7 K. The lower inset shows the disappearance of the Meissner signal in iron when the pressure is decreased to 3.5 GPa in the b.c.c. phase.

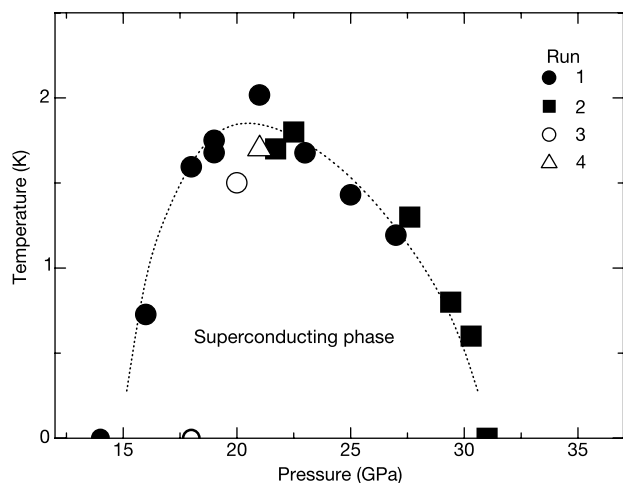


Figure 4 Superconducting phase diagram of iron. The transition temperature, T_c , is defined by the onset of the transition. The dashed curve is a guide for the eye. T_c values shown by black circles and squares (runs 1 and 2) are obtained from electrical resistance measurements with sodium chloride as a pressure medium. Run 3 (white circle) is a run without a pressure medium while releasing the pressure from 90 GPa. Run 4 (white triangle) shows the onset of the Meissner signal in the magnetization measurement. T_c appears at around 15 GPa and increases with pressure. T_c reaches the maximum value of 2 K at around 21 GPa and vanishes above 30 GPa.

of the total residual resistivity. This is because the residual resistivity includes contributions from the thin gold wire in series with the sample as well as from the finite contact resistance, which is estimated to be around 90% of the measured resistance. The main impurities contained in the starting material were O, Ta, Si and Co at concentrations of 115, 10, 8.3 and 8.3 p.p.m., respectively, according to the chemical analysis data. Thus we regard the drop as the onset of superconductivity of iron.

To confirm the superconductivity, we tried to detect the Meissner effect using a SQUID (superconducting quantum interference device) magnetometer at 21 GPa. A 4:1 mixture of methanol/ethanol was used as the pressure-transmitting medium. An iron sample was obtained from the rod that provided the samples used for the resistance measurements, cut into slices 0.04 mm in thickness and 0.15 mm in diameter, and placed in the chamber of the BeCu gasket. Several turns of pick-up coil for the SQUID magnetometer were wound closely around the pressure surface of the diamond and an equal number of turns near to the diamond for background compensation. A small tin chip was put inside the compensation coil as a reference sample to check both the sign and the magnitude of the signal from iron. Figure 3 shows the superconducting transition signals from iron at 1.7 K and tin at 2.7 K, of opposite sign.

The pressure dependence of the transition temperature T_c was observed in the pressure range between 15 GPa and 30 GPa (Fig. 4). Superconductivity was observed in three different runs of the resistivity measurements and the magnetization measurement. Runs 1 and 2 were obtained by quasi-hydrostatic conditions with NaCl as the pressure-medium. No pressure-medium was used for run 3 and the superconductivity transition was observed only while reducing the pressure from 90 GPa. This implies that even a very small amount of remaining ferromagnetic b.c.c. iron may suppress the onset of superconductivity and that its transformation to h.c.p. iron is caused by either quasi-hydrostatic pressure or by increasing the pressure as much as possible. We conclude that the superconducting phase of iron appears after the establishment of the non-magnetic state at 15 GPa, which is close to the beginning of the b.c.c.-to-h.c.p. structural transition of iron. □

Received 29 January; accepted 25 May 2001.

1. Cort, G., Taylor, R. D. & Willis, J. O. Search for magnetism in hcp ϵ -Fe. *J. Appl. Phys.* **53**, 2064–2065 (1982).
2. Taylor, R., Pasternak, M. & Jeanloz, R. Hysteresis in the high pressure transformation of bcc- to hcp-iron. *J. Appl. Phys.* **69**, 6126–6128 (1991).
3. Wohlfarth, E. P. The possibility that ϵ -Fe is a low temperature superconductor. *Phys. Lett. A* **75**, 141–143 (1979).
4. Freeman, A. J., Continenza, A., Massida, S. & Grossman, J. C. Structural and electronic properties and possible superconductivity in simple cubic Fe. *Physica C* **166**, 317–322 (1990).

Acknowledgements

We thank T. C. Kobayashi for stimulating discussion. This work has been supported by a Grant-in-Aid for COE (Center of Excellence) Research and Scientific Research from the Ministry of Education, Culture, Sports, Science and Technology in Japan, and also by Core Research for Evolution Science and Technology of the Japan Science and Technology Corporation.

Correspondence and requests for materials should be addressed to K.S. (e-mail: kshimizu@mp.es.osaka-u.ac.jp).

Direct observation of hole transfer through DNA by hopping between adenine bases and by tunnelling

Bernd Giese, Jérôme Amaudrut, Anne-Kathrin Köhler, Martin Spormann & Stephan Wessely

Department of Chemistry, University of Basel, St Johannis Ring 19, CH-4056 Basel, Switzerland

The function of DNA during oxidative stress¹ and its suitability as a potential building block for molecular devices^{2–4} depend on long-distance transfer of electrons and holes through the molecule, yet many conflicting measurements of the efficiency of this process have been reported^{5,6}. It is accepted that charges are transported over long distances through a multistep hopping reaction^{7–11}; this ‘G-hopping’⁸ involves positive charges moving between guanines (Gs), the DNA bases with the lowest ionization potential. But the mechanism fails to explain the persistence of efficient charge transfer when the guanine sites are distant^{7,12}, where transfer rates do not, as expected, decrease rapidly with transfer distance. Here we show experimentally that the rate of charge transfer between two guanine bases decreases with increasing separation only if the guanines are separated by no more than three base pairs; if more bridging base pairs are present, the transfer rates exhibit only a weak distance dependence. We attribute this distinct change in the distance dependence of the rate of charge transfer through DNA to a shift from coherent superexchange charge transfer (tunnelling) at short distances to a process mediated by thermally induced hopping of charges between adenine bases (A-hopping) at long distances. Our results confirm theoretical predictions of this behaviour^{13–17}, emphasizing that seemingly contradictory observations of a strong^{8,9} as well as a weak^{7,12} influence of distance on DNA charge transfer are readily explained by a change in the transfer mechanism.

We have measured the efficiency of the charge transfer between Gs, separated by adenine-thymine (A-T)_n bridges of various lengths, in double strands 1a–h (Fig. 1). Photolysis of the 4'-acylated nucleotide in DNA 1 generates the sugar radical cation in 2 (Fig. 1), which injects a positive charge into G₂₂ of the complementary, radiolabelled strand (2→3; Fig. 1). This guanine radical cation G₂₂⁺ is either trapped irreversibly by water, yielding after piperidine treatment the strand cleavage product P_G, or it induces an electron